ECS Transactions, 64 (2) 191-199 (2014)
10.1149/06402.0191ecst ©The Electrochemical Society

Electrode/Electrolyte Interphase Studies of Ceria Based Electrolytes for IT-SOFCs

L. Baqué[a], K. Padmasree[b], A. F. Fuentes[b], A. Serquis[a], and A. Soldati[a],

[a] CONICET, CAB-CNEA, Av. Bustillo 9500, (8400) Bariloche, Argentina
[b] Cinvestav Unidad Saltillo, Apartado Postal 663, CP 25000, Saltillo, Mexico

Solid oxide fuel cells (SOFCs) require high operation temperatures (up to 800°C) in order to allow oxygen ion conduction through the ceramic electrolyte. Lowering SOFC operation temperature implies enhancing the transport and electrochemical properties of both electrolyte and cathode. In this work, the electrochemical performance of nanostructured $La_{0.4}Sr_{0.6}Co_{0.8}Fe_{0.2}O_{3-d}$ (LSCFO)/$Ce_{0.8}Gd_{0.2}O_{2-d}$(CGO)/LSCFO and LSCFO/$Ce_{0.8}Nd_{0.2}O_{2-d}$ (CNO)/LSCFO symmetrical cells was investigated. The bulk conductivity is similar for both electrolytes, while the grain boundary and total conductivities are higher for the CGO electrolyte. Nevertheless, CGO electrolyte exhibits large pores that compromise its mechanical properties. In addition, cathode performance degrades in LSCFO/CGO/LSCFO cells.

Introduction

A solid oxide fuel cells (SOFC) is considered as a highly efficient power generation system due to its high performance, low environmental impact, high waste heat utilization and fuel flexibility (1,2). A conventional SOFC uses 8 mol% yttria stabilized zirconia (YSZ) as electrolyte. YSZ electrolyte exhibits high oxygen ion conductivity and chemical stability in oxidizing and reducing atmospheres, but its operating temperature is high (around 800°C). The necessity of this high operating temperature has resulted in high cost, physical and chemical degradation of the component materials. Therefore, there is a continuous search for alternative materials which can be used as electrolyte for intermediate temperature (IT) operation in the 500-800°C temperature range. Many studies have been made on various electrolyte materials for the IT-SOFC, such as gadolina doped ceria, samaria doped ceria, scandia stabilized zirconia, strontium and magnesium co-doped lanthanum gallate (2). Among these, doped ceria has been considered as one of the most promising electrolyte materials for intermediate temperature operation of SOFC (1) due to their higher ionic conductivity with respect to doped zirconia and to their lower cost with respect to lanthanum gallate based materials.

Ceria is a fluorite structured ceramic material (space group Fm3m) that can be readily doped with a variety of aliovalent (alkaline earth or rare earth) cations to form solid solutions. When so doped, oxygen vacancies are introduced into the CeO_2 lattice for charge compensation and the materials become good ionic conductors for a variety of electrical applications. Conventionally, ceria based materials are synthesized at high temperatures. Several chemical techniques (hydrothermal synthesis, co-precipitation, decomposition of oxalate precursors, molten salt etc.) have been adopted for obtaining

uniform ultrafine non-agglomerated ceria and doped ceria particles. They present a higher specific area and can be more easily compacted and sintered than conventional powders.

Conduction in ceramic electrolyte can occur through the bulk and/or the grain boundary paths (3). Consequently, the evaluation of the electrolyte bulk and the grain boundary conductivities plays an important role in the optimization of its transport properties. In general, this task is accomplished by using the electrochemical impedance spectroscopy (EIS) technique but these two components can be only accurately separated at temperatures down below SOFC operation temperature (i.e. < 500°C). Cathode overpotential is usually high at these temperatures and hence Pt electrodes are used for such evaluation. However, the SOFC performance depends not only on the individual performance of each cell component but also on their interphase (4,5). In the last years, high performance SOFC cathodes have been developed by using mixed conductor materials and by optimizing its microstructure (6). These cathodes not only improve the cell performance but also allow the evaluation of the electrolyte bulk and grain boundary conductivities using real SOFC cathodes. In this work, we present the evaluation of the microstructural and electrochemical properties of two symmetrical cells: $La_{0.4}Sr_{0.6}Co_{0.8}Fe_{0.2}O_{3-d}$ (LSCFO)/$Ce_{0.8}Gd_{0.2}O_{2-d}$(CGO)/LSCFO and LSCFO/$Ce_{0.8}Nd_{0.2}O_{2-d}$ (CNO)/LSCFO. Nanostructured LSCFO powders were synthetized by an acetate based method (6) and then deposited on CGO and CNO substrates by spin coating. CGO and CNO electrolytes were produced by a molten salt route (7). Microstructural properties were investigated by scanning electron microscopy (SEM) and the electrochemical performance of electrolytes, cathodes and cathode/electrolyte interphases were evaluated by EIS.

Experimental

$Ce_{0.8}Gd_{0.2}O_{2-d}$ and $Ce_{0.8}Nd_{0.2}O_{2-d}$ powders were prepared by a two-step method comprising a mechanically induced metathesis reaction followed by short firing at temperatures above sodium nitrate's melting point (7). The starting materials used were high purity (Aldrich, >99+ %) analytical grade cerium nitrate, neodymium nitrate and sodium hydroxide. The nitrates were weighed according to the stoichiometry and mixed with appropriate amount of NaOH, and dry milled together for 30 min in a planetary ball mill by using yttria partially stabilized zirconia (5.2wt% Y_2O_3) containers (volume 125 ml) and balls (20 mm diameter), balls to powder mass ratio = 10:1) at a rotating disc speed of 350 rpm. The amount of the reactant was salt balanced such that there was no alkali metal or nitrate excess. The resulting activated precursor material was dried for 1 h at 120°C to reduce moisture and minimize violent gas evolution on melting. The precursors were then loaded in to alumina crucibles and fired in air for 3 h either at 350 or 500°C using an electrical furnace (Carbolite, heating rate 5°C) and cooled thereafter to room temperature. The solidified melt obtained was washed with distilled water to remove the soluble $NaNO_3$ by product whereas the solid residue was collected by centrifugation. This step was repeated until no traces of NO_3^- ions were detected. Doped ceria powders were uniaxially pressed to form pellets and then sintered at 1500°C for 6 h. The obtained substrates were ~ 1.3 mm thick.

$La_{0.4}Sr_{0.6}Co_{0.8}Fe_{0.2}O_{3-d}$ (LSCFO) powders were prepared by acetic acid-based method. Detailed preparation procedure and microstructural characterization of these cathodes

were reported elsewhere (6). These powders were dispersed in an ink and deposited onto both sides of CGO and CNO substrates by the spin coating technique. Afterwards, these assemblies were heat treated at 900°C, resulting in a symmetrical cell configuration used for electrochemical measurements. Cathode covered all the electrolyte surface reaching a geometric area of 0.8-0.9 cm^2.

Impedance measurements were performed in the 300-600°C temperature range under pure oxygen. The temperature was raised from 375°C up to 600°C and then cooled down to 300°C. Impedance spectra were recorded using a potentiostat/impedance analyzer Autolab (Eco Chemie BV) within the 10^{-3}-10^{6} Hz frequency range. A stabilization time of at least 3 h elapsed before each EIS measurement. Platinum grids, slightly pressed on electrodes, were used as current collectors. Electrolyte and cathode microstructure was characterized by SEM.

Results and discussion

Electrochemical impedance spectroscopy

Figure 1 shows a typical impedance spectrum measured under pure oxygen at 300°C corresponding to the LSCFO/CNO/LSCFO cell. A small part of an arc can be distinguished at the highest frequencies, while two complete arcs can be identified at intermediate and low frequencies. All spectra were fitted with the equivalent circuit shown in the inset of Figure 1. The series resistance R_{Bulk} represents the intersection of the arc partially observed at the highest frequencies and it is related to the conduction through the electrolyte bulk. The intermediate frequency arc was fitted with a sub-circuit composed of the resistance $R_{Grain\ Boundary}$ in parallel with the constant phase element $CPE_{Grain\ Boundary}$, being this contribution related to the conduction through the electrolyte grain boundaries. The low frequency arc represents the oxygen reduction reaction (ORR) at the cathode, including the O^{2-} transfer through the cathode/electrolyte interphase. This contribution was fitted using the impedance $Z_{Cathode}$.

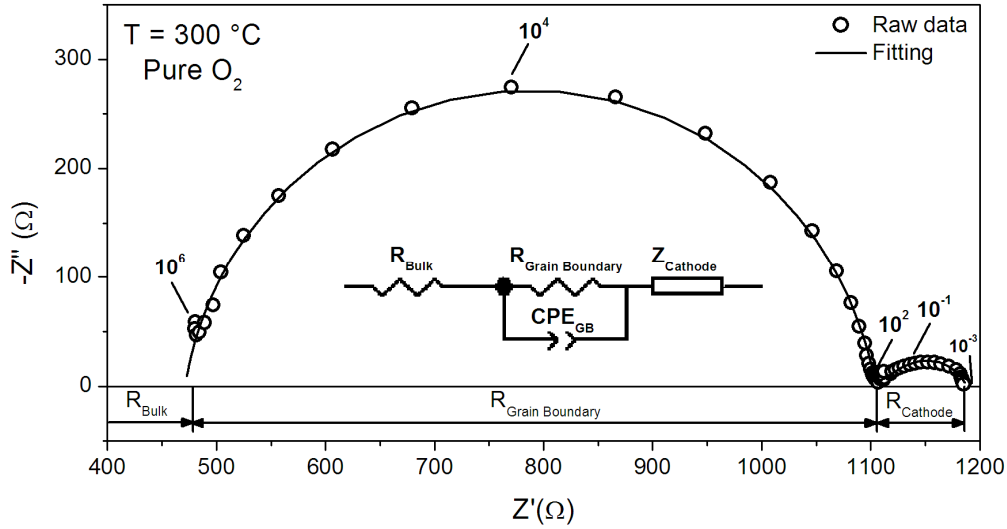

Figure 1. Nyquist plot of an EIS spectrum recorded under pure O_2 at 300°C for the LSCFO/CNO/LSCFO symmetric cell. The numbers indicates the frequency in Hz.

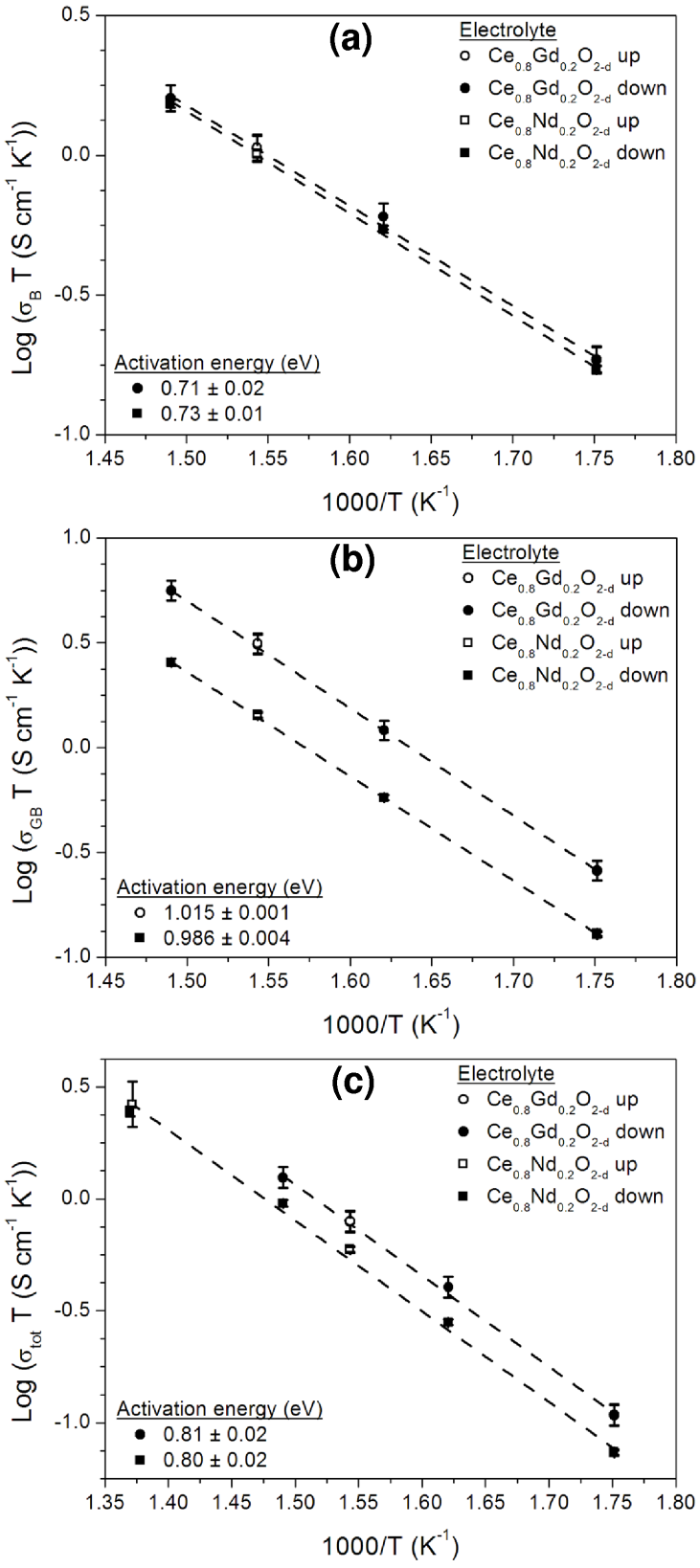

Figure 2. Arrhenius plot of the (a) bulk, (b) grain boundary and (c) total conductivity values measured under pure oxygen for CGO and CNO electrolytes. The dotted lines represent the linear fitting of values.

Bulk, grain boundary and total electrolyte conductivities can be estimated by using the expression $\sigma = L/(R \cdot A)$ where σ is the conductivity, L is the electrolyte thickness, R is the resistance (estimated by fitting the EIS spectra as explained above), and A is the electrolyte area. Arrhenius plots of the bulk, grain boundary and total conductivities for CGO and CNO electrolytes are displayed in Figure 2. Both electrolytes exhibit similar bulk conductivity values, while grain boundary conductivity values are higher for CGO electrolyte by a factor of 2. As a consequence, total conductivity is also higher for CGO but by a factor of ~1.5. Activation energy values are similar for both electrolytes. It is worth to note the good consistency between the conductivity values measured while the temperature was raised (denoted as *up* in the graph) and the values measured during the cooling down (denoted as *down* in the graph).

Cathode area specific resistance ($ASR_{cathode}$) values were evaluated by using the equation $ASR_{cathode} = R_{cathode} \cdot A$ where $R_{cathode}$ is the real component of $Z_{cathode}$ and A is cathode geometric area. The corresponding Arrhenius plot can be seen in Figure 3. The values denoted as *up* were recorded during the heating while the values denoted as *down* were measured during cooling. The LSCFO/CGO/LSCFO cell has slightly lower $ASR_{cathode}$ values than LSCFO/CNO/LSCFO cell during heating. However, $ASR_{cathode}$ values increase during cooling for the LSCFO/CGO/LSCFO cell. In contrast, LSCFO/CNO/LSCFO cell values recorded during cooling are consistent with those measured during heating.

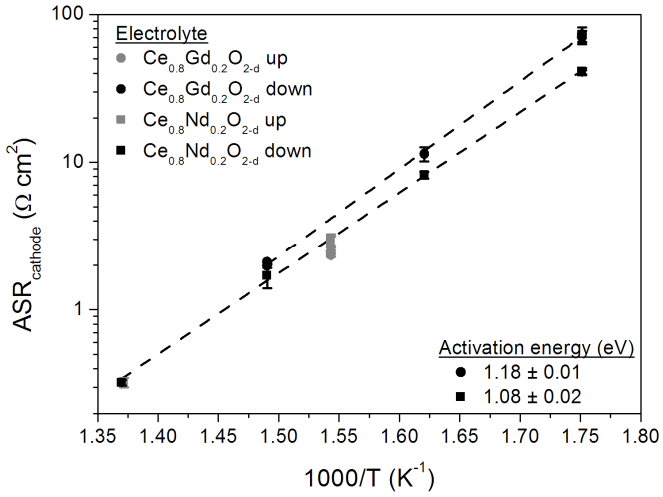

Figure 3. Arrhenius plots of the total ASR values measured under pure oxygen for LSCFO cathodes deposited on CGO and CNO electrolytes. The dotted lines represent the linear fitting of values.

The cathode contribution of the EIS spectra was fitted by using a Warburg element (8) in the case of the LSCFO/CNO/LSCFO cell. The same model was applied for the LSCFO/CGO/LSCFO spectra recorded during heating, but an R//CPE sub-circuit had to be added for fitting spectra measured during cooling. This fact can be appreciated in the Bode plot shown in Figure 4. The cathode contribution part is similar in EIS spectra measured during heating and cooling for the LSCFO/CNO/LSCFO cell, and during heating for the LSCFO/CGO/LSCFO cell. However, an additional contribution becomes apparent at the lowest frequencies in the EIS spectrum measured during cooling for the LSCF/CGO/LSCFO cell. Therefore, the cathode degradation effect in the

LSCFO/CGO/LSCFO cell observed after thermal treatment is due to an additional ORR limiting step.

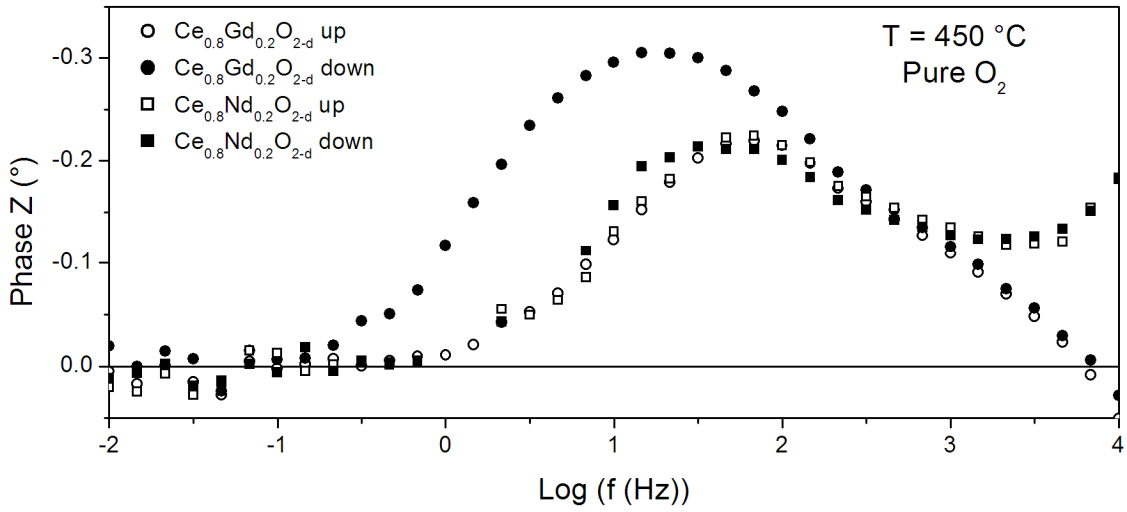

Figure 4. Bode plot of the impedance spectra recorded under pure oxygen at 450°C for the LSCFO/CGO/LSCFO and LSCFO/CNO/LSCFO symmetric cells when raising (up) and decreasing (down) the temperature.

Electrochemical properties of electrolytes, cathodes and cathode/electrolyte assemblies depend not only on their composition but also on their microstructure. In view of that, the microstructural characterization is reported in the next section.

Scanning electron microscopy

SEM images of the CGO and CNO electrolyte surfaces before the deposition of the cathode show some differences between them (see Figure 5a and c). The CGO electrolyte is composed of larger grains with a broader particle size distribution (reported in Figures 5b and d). In addition, CGO grains look more connected than those of the CNO electrolyte. Electrolytes with smaller grain sizes contain more grain boundaries. Conduction through grain boundaries is, in principle, faster than in bulk (9). Therefore, it is a priori expected that electrolytes with smaller grain sizes exhibit higher grain boundary conduction. Nevertheless, several factors can negatively influence conduction through grain boundaries. A typical example is the presence of impurities that tend to segregate at grain boundary hindering the conduction (10). In the case of the CNO electrolyte studied here, it is apparent that the poor connectivity between grains is the main cause of the lower grain boundary conductivity.

The porosity of the electrolyte is another important factor that influences the conductivity and the mechanical integrity of electrolyte substrates. According to Figures 5a and c, pore sizes are similar for both CGO and CNO electrolytes but the CNO electrolyte presents a larger number of them. However, cross-section SEM images shown in Figures 6a and b give a different impression. At this scale, CNO electrolyte looks dense while CGO substrate presents considerable large pores. Images acquired with higher magnification allow observing electrolyte microstructure in more detail (see Figures 6c and d). The CNO electrolyte have rounded and closed pores. The CGO

electrolyte has, in addition, channel-like pores; although they do not penetrate the substrate from side to side. The effect of these pores on the CGO electrolyte conductivity seems to be limited, but they would compromise the mechanical properties of the substrate. In fact, the LSCFO/CGO/LSCFO cell was unintentionally broken during mounting for SEM analysis likely because of its higher brittleness.

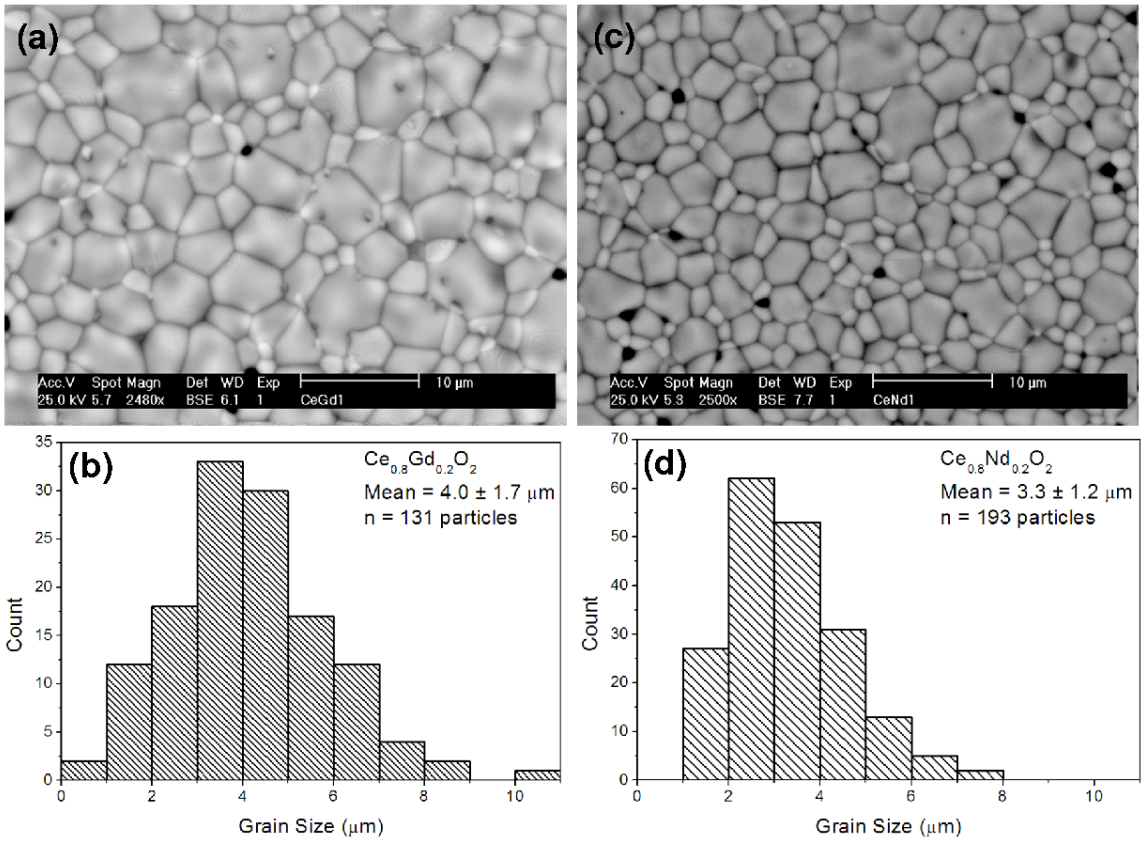

Figure 5. SEM images of the (a) CGO and (c) CNO electrolyte surfaces before cathode deposition. Scale bar indicates 10 µm. Particle size distribution of (b) CGO and (d) CNO electrolytes.

The cathode microstructure after EIS measurements is similar for both LSCFO/CGO/LSCFO and LSCFO/CNO/LSCFO cells (see Figures 6c and d). Cathode thickness is roughly 3-4 µm. The cathode/electrolyte interface shows good contact between them in both cells. No evident signs of cathode degradation were observed for LSCFO/CGO/LSCFO cell. X-ray diffraction patterns (not shown) collected at the cathode surface did not reveal any sign of degradation either. It is important noting that both cathodes were prepared from the same powder batch. Moreover, the preparation of the symmetrical cells and the EIS measurements were performed using the same setup simultaneously. Therefore, it is highly probable that the cathode degradation observed in the LSCFO/CGO/LSCFO cell was originated from the cathode/electrolyte interaction instead of being produced by an external source. Cathode performance degradation can be caused by chemical reaction between the electrode and the electrolyte. However, in some cases, reaction products are hardly detected by conventional characterization techniques such as X-ray diffraction (5). The FIB/lift-out technique allows obtaining site-specific samples from cathode/electrode interphase suitable for transmission microscopy

analysis even at atomic scale (4,5). Accordingly, sample preparation by FIB/lift-out technique and the study of the LSCFO/CGO interphase is planned for the near future in order to elucidate the origin of cathode degradation.

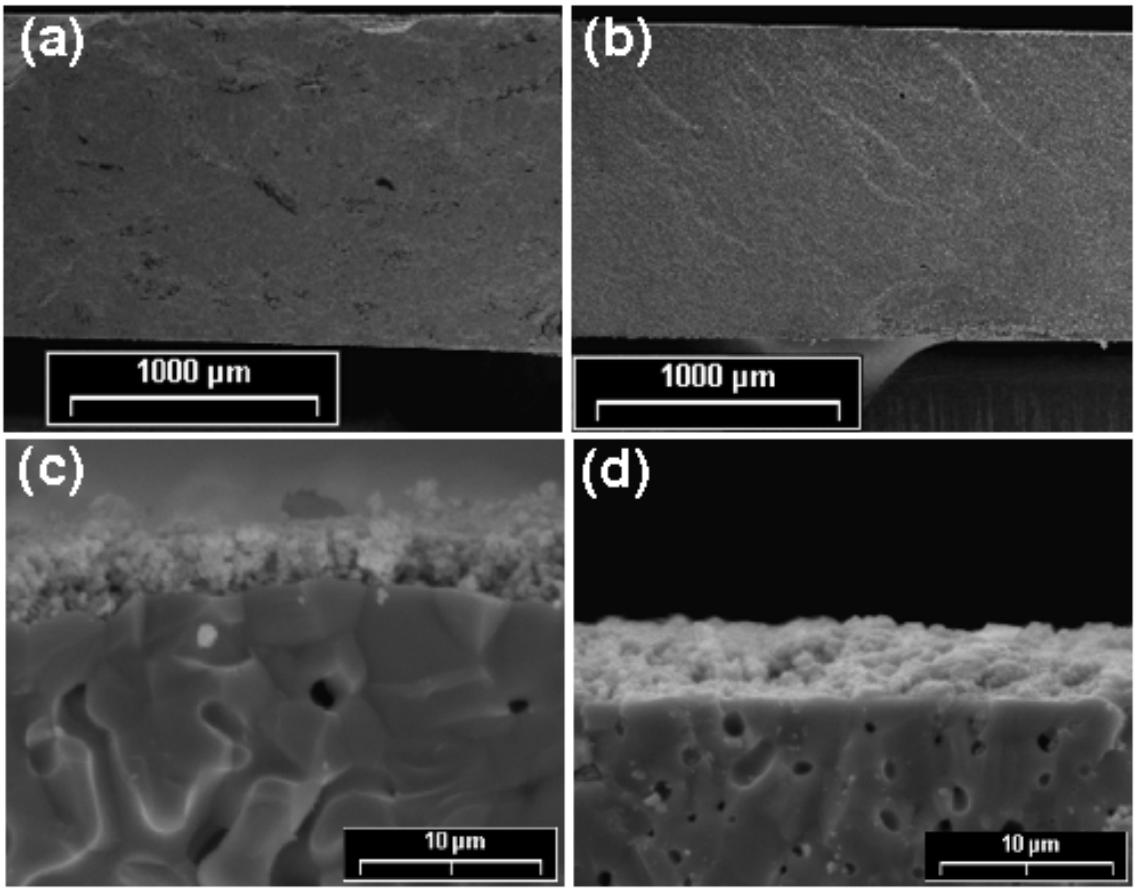

Figure 6. Cross-section SEM images of (a,c) LSCFO/CGO/LSCFO and (b,d) LSCFO/CNO/LSCFO cells. The cathode is on top and the electrolyte is at the bottom in (c) and (d). The images were acquired after EIS measurements.

Even though CGO electrolytes exhibit better transport properties than CNO electrolytes, the former also present poor mechanical properties and produces the degradation of the cathode performance. These facts are undesirable since they would influence negatively the entire SOFC. Therefore, the CNO electrolyte shows better properties for its use as electrolyte along with nanostructured LSCFO cathodes.

Conclusions

The electrochemical and microstructural properties of LSCF/CGO/LSCFO and LSCFO/CNO/LSCFO symmetrical cells were evaluated. CGO electrolyte exhibits grain boundary and total conductivity values ~ 2 and 1.5 times higher than those of the CNO electrolyte, respectively. The bulk conductivity is similar for both electrolytes. However, the LSCFO/CGO/LSCFO cell has a porous electrolyte with poor mechanical properties and also presents cathode performance degradation after thermal cycling up to 600°C. Both of them are highly detrimental for SOFC operation. These findings reinforce the

concept that SOFC performance depends not only on the performance of each individual cell component but also on the interaction between them.

Acknowledgments

This work is part of a bilateral collaboration project between Argentina and Mexico which was funded by CONICET-CONACYT (funding D1765). It was also funded by University of Cuyo, CNEA and ANPCyT-PICT.

References

1. B. C. H. Steele and A. Heinzel, *Nature*, **414**, 345 (2001).
2. A. J. Jacobson, *Chem. Mat.*, **22**, 660 (2010).
3. S. Kim and J. Maier, *J. Electrochem. Soc.*, **149**, J73 (2002).
4. A. L. Soldati, L. Baqué, H. Troiani, C. Cotaro, A. Schreiber, A. Caneiro and A. Serquis, *Int. J. Hydrogen Energy*, **36**, 9180 (2011).
5. A. Montenegro-Hernández, A. Soldati, L. Mogni, H. Troiani, A. Schreiber, F. Soldera and A. Caneiro, *J. Power Sources*, **265**, 6 (2014).
6. L. Baqué, A. Caneiro, M. S. Moreno and A. Serquis, *Electrochemistry Comm.*, **10**, 1905 (2008).
7. E. Mendoza-Mendoza, K. Padmasree, S. Montemayor and A. Fuentes, *J. Mater. Sci.*, **47**, 6076 (2012).
8. N. Grunbaum, L. Dessemond, J. Fouletier, F. Prado, L. Mogni and A. Caneiro, *Solid State Ionics*, **180**, 1448 (2009).
9. P. Heitjans and S. Indris, *J. Phys.: Condens. Matter*, **15**, R1257 (2003).
10. T. S. Zhang, J. Ma, H. Cheng and S. H. Chan, *Mater. Res. Bull.*, **41**, 563 (2006).